Section 2
ADVANCED TECHNOLOGY DEVELOPMENTS

2.A Studies of New Geometries for X-Ray Lasers

Laser-produced plasmas have been extensively used as suitable media for soft x-ray lasers. Recently, amplified spontaneous emission at the 130-Å to 200-Å range has been observed in experiments involving laser-produced plasmas.[1-3] Gain coefficients of about 5 to 6 cm^{-1} were measured on $2s^22p^53s - 2s^22p^53p$ transitions in neon-like selenium, yttrium, and molybdenum. In the lasing scheme used in these experiments, free electrons in the laser-produced plasma collide with neon-like ions, exciting $2p$ electrons to the $3p$ and $3s$ states (see Fig. 30.11). The $3s$ state decays to the ground level much faster than the $3p$ state, creating a population inversion between the $3s$ and $3p$ states.[4] Stimulated x-ray emission, initiated by slower spontaneous decay from the $3p$ to the $3s$ state, propagates and is amplified along the axis of the plasma (typically 1- to 3-cm long).

In x-ray laser schemes, the target and the irradiating laser parameters should be chosen to maximize population inversion and therefore gain. The gain coefficient depends mainly on the plasma temperature and density and on the nuclear charge Z of the target material. The temperature (which in turn depends on the incident laser irradiance) determines the various atomic rates and the fraction of neon-like ions. For a given neon-like ion fraction, the gain increases with the plasma electron density until that density is high enough to allow electron collisions to equilibrate the level populations, thus reducing the population inversion and therefore the gain. The electron density corresponding to the peak gain increases with the nuclear

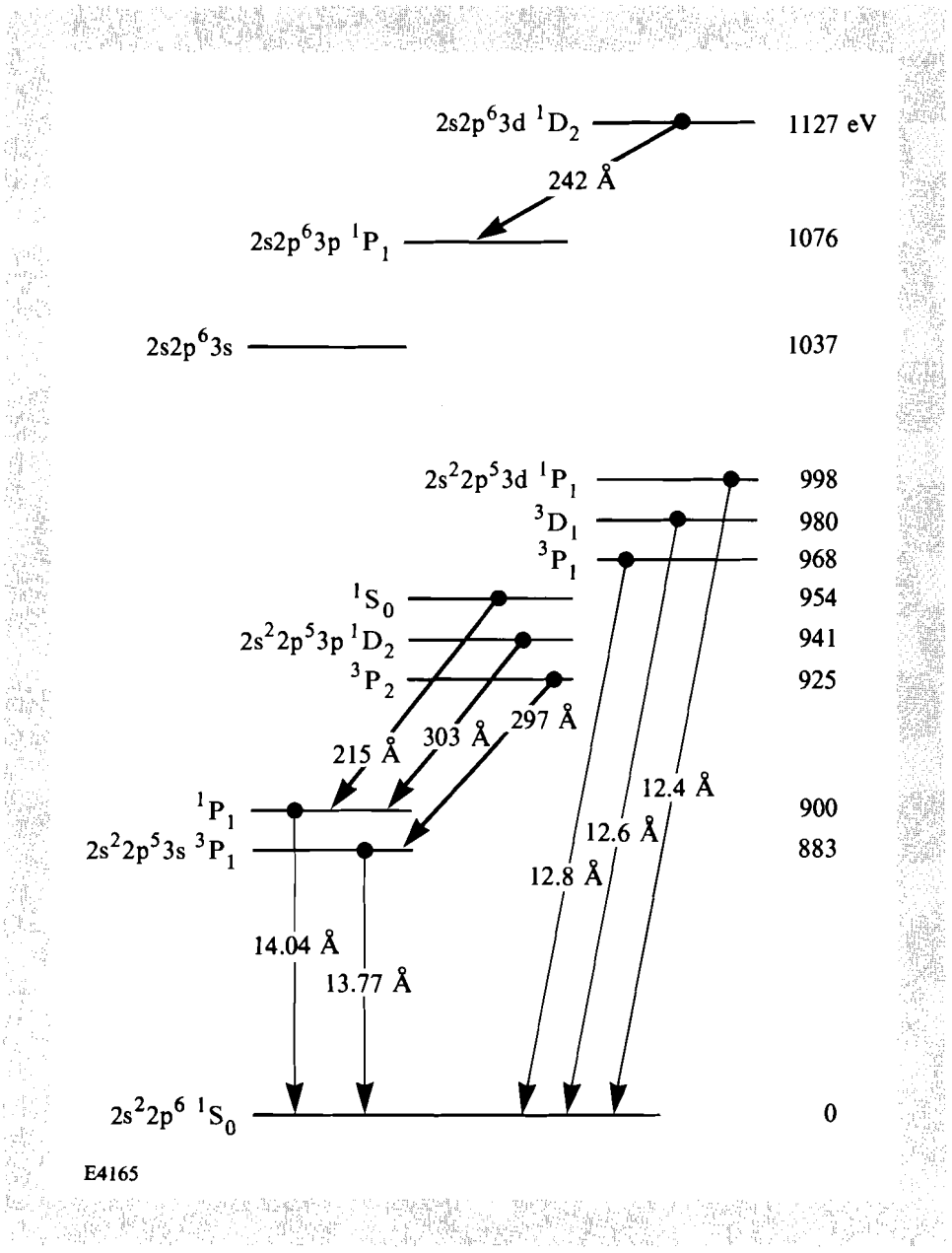

Fig. 30.11
The x-ray and XUV transitions in Ne-like nickel. The XUV transitions that are expected to exhibit gain are emphasized. The five $n=3$ to $n=2$ x-ray lines shown are those used to diagnose the fraction and spatial extent of Ne-like ions in the plasma.

charge Z; it is about 10^{21} cm^{-3} for iron ($Z = 26$) and 10^{22} cm^{-3} for krypton ($Z = 36$).[5] For a given density, the gain initially increases sharply with increasing nuclear charge Z, then decreases slowly. Thus, for each density value there is an optimal Z.

It should be mentioned that for lower-Z plasmas, the opacity of the $2s$-$2p$ transitions transverse to the lasing direction is higher and has to be more carefully controlled since it can reduce the gain by increasing the population of the lower laser level.

We chose nickel as the lasing medium because, for the density range attained in these experiments (in the mid-10^{20} cm^{-3}), it yields a gain coefficient close to optimal. Also, nickel requires only modest plasma

temperatures (500 to 700 eV) as compared with a higher-Z target. This temperature is compatible with the laser intensity available for these experiments. For lower-Z ions, the lower laser power dictated by the requirement of a lower temperature may be inadequate for achieving burn-through and desirable density profile characteristics. Choosing nickel (rather than selenium) leads to longer-wavelength lasing lines, in the range 215 to 300 Å, as compared with 180 to 210 Å for selenium. Since the optimal plasma density (even for nickel) is higher than that occurring in simple exploding-foil experiments, we have concentrated on new target geometries that can increase the plasma density and lead to higher gain.

In previous x-ray laser experiments,[1-3] thin exploding targets were used to avoid the steep density gradient characteristic of plasma expansion from thick targets. The thin target explodes and generates a roughly cylindrical plasma having a flat electron density profile of about $3\text{–}5 \times 10^{20}$ cm^{-3}, and a flat temperature profile. Since the lateral scale length is of the order of 100 to 150 μm, the refraction effect is reduced, and rays can now propagate 1 to 2 cm in such a profile before being deflected out of the lasing region.

The exploding foil geometry suffers from two drawbacks: first, in order to achieve a symmetrically expanding plasma with a long scale length, the laser must burn through the foil before the peak of the laser pulse. Consequently, the electron density at the time of lasing is only about 4×10^{20} cm^{-3}. This is lower than the density for maximum gain coefficient by at least a factor of 2. Second, the refraction effect, which was reduced by employing the exploding foil geometry, still limits the length of the plasma column to 1 to 3 cm because the density profile tapers away from the axis. In the new geometries described here, an attempt is made to overcome these limitations. These geometries, in addition to increasing the density, may also result in a wider lasing channel and a concave lateral density profile, both of which reduce refraction losses.

In the following section we introduce these new geometries and discuss their expected performance. We then present experimental results, accompanied by computer simulations, and discuss their relevance to future x-ray laser experiments.

New Geometries: Theoretical Considerations

1. Two Exploding Foils

The density profile of a single, thin, exploding nickel foil is shown schematically in Fig. 30.12(a). After the initial burn-through, a nearly symmetrical expansion, with a Gaussian density profile, is obtained. A population inversion is achieved early, but the lasing x rays suffer severe refraction losses until the plasma has reached large enough lateral dimensions. Since the optimal temperature for lasing in neon-like nickel is about 600 eV (compared with about 1 keV for selenium), a lower irradiance is used. This leads to a lower ablation rate and dictates using a thinner foil. A thinner foil, in turn, leads to a smaller density scale length. For single-foil geometry, the only way to overcome this drawback is to employ much longer laser pulses with thicker foils.

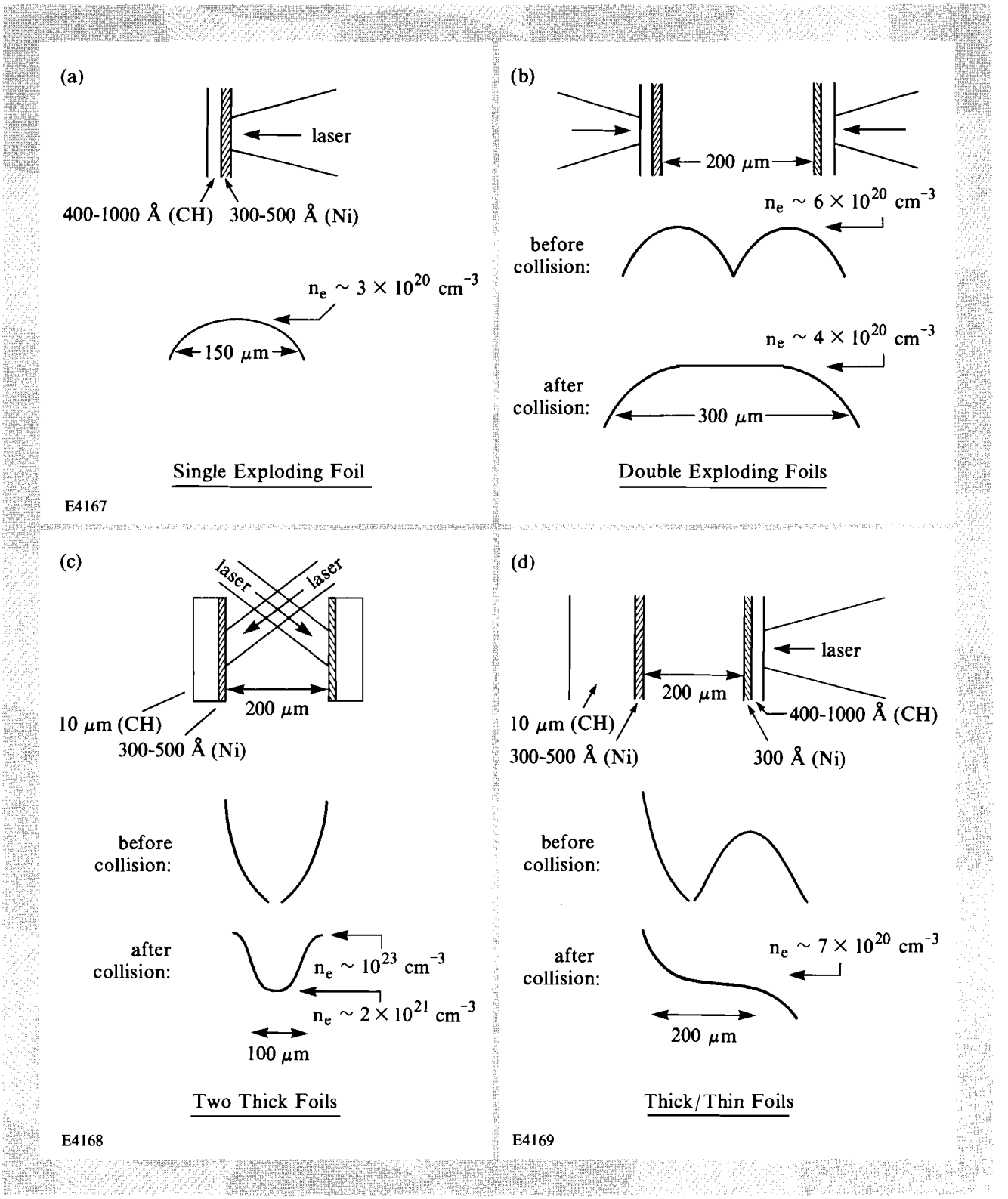

Fig. 30.12
The conceptual spatial density profile behavior of several target configurations discussed in this report: (a) single exploding foil; (b) double exploding foil; (c) two thick foils; and (d) a combination of one thick and one thin foils.

An improved arrangement is that of two parallel foils facing each other[6] as shown in Fig. 30.12(b). This is in contrast to a recently suggested geometry in which the foils are placed next to each other along their edges (thus forming a slit),[7] rather than facing each other. In the former geometry, the lasing medium is formed by the bulk of the expanding plasma, while in the slit geometry it is formed only from the plasma created on the slit edges. The optimal distance between the exploding foils was found to be about 150 to 250 μm, for an irradiance of the order of 10^{13} W/cm^2. For much larger distances, the collision between the two plasmas occurs when the density has fallen to too low a level for lasing, whereas for much smaller distances the increase in scale length over the single-foil case is not significant.

The arrangement of two exploding foils offers the following advantages: first, when the plasmas expand inward from the two foils and begin to collide, a concave density profile having a dip at the midplane is formed. Later on, the profile is flat topped with a greater width than in the corresponding single-foil case. Additionally, we have found that a pair of thin foils can be irradiated from only one side and still result in density profiles similar to the case where a double foil is irradiated from both sides. In such a design, the laser burns through the first foil prior to the peak of the pulse; it is then transmitted through the first-foil plasma and absorbed by the second foil, causing it to explode. A uniform plasma can be formed between the foils even though the interface between the two colliding plasmas will not be on the midplane. The thicknesses of the two foils can be optimized in order to produce more uniform temperature and density profiles. This requires that the energy absorbed in the second foil be higher than that absorbed in the first foil to compensate for the time delay between the two foil explosions. The related geometry of imploding thin cylindrical shells has been previously studied at the Laboratory for Laser Energetics, theoretically and experimentally.[8] In the cylindrical geometry, the effects of widening the density profile and making it concave apply in both transverse dimensions, rather than in only one of them. However, the cylindrical geometry requires a large number of beams, appropriately positioned to provide uniform illumination of the target.

2. Two Ablating Slabs

The arrangement of two exploding foils does not result in significantly higher plasma density as compared with the single-foil case. This is because when the two foils collide they both are expanding outward. Since the mass is limited in each foil, there is no hydrodynamic support from the two exploding plasmas, and the maximum pressure occurs in the collision region; this leads to a rapid disassembly of the system. To meet the goal of achieving higher density we have designed a novel geometry, consisting of two slabs (thick foils) irradiated on their inner surfaces that face each other [Fig. 30.12(c)]. Since the laser does not burn through these thick foils, the resulting density profile falls sharply from either foil toward the midplane. A concave profile with a minimum between the slabs is formed. The ablated material, which is now hydrodynamically confined between the slabs, reaches densities throughout the pulse about a factor of 10 to 100 times higher than those attained in the

exploding-foil geometries. The slab separation can be chosen to yield the optimal density for an extended period of time. A much higher x-ray laser gain can be obtained with this geometry, compared to that of the exploding foils, because of the higher, more optimal density that is achieved and because of the collimating effect of a concave density profile. In this geometry, rays traveling in an off-axis direction will be refracted back into the lasing medium rather than out of it, as in the convex density profile of an exploding foil. The higher density may adversely affect lasing if the transverse opacity of transitions to the ground state becomes much higher than 1. The high opacity repopulates the lower level of the lasing transition, leading to a reduction in the population inversion. This effect can be particularly severe because the stagnated plasma lacks a velocity gradient that could mitigate the effect of opacity (through the Doppler shift). To remedy this problem, the two foils can be made from thin layers of the lasing material deposited on a thick substrate. The substrate material will provide the hydrodynamic confinement and wave guiding without contributing to the population of the lower laser level via resonant excitations.

3. A Pair of Exploding/Ablating Foils

As in the case of the two thin foils, we have found a simpler version of the geometry of two ablative slabs that retains some of the advantages of that particular geometry. In this simplified version, a thin foil is placed in front of a thick foil and is irradiated by a single laser beam [Fig. 30.12(d)]. The laser irradiates the thin foil, burns through it before the peak of the pulse, and then irradiates the thick foil. The collision between the plasmas of the exploding thin foil and ablating thick foil forms a plateau on the falling density profile of the thick foil. The resulting density is higher than that attained in exploding-foil plasmas. The scale length of this plateau is about equal to the original foil separation. The advantage of high density, inherent in the thick-foil case, is partially retained. However, the advantage associated with a concave density profile is retained now only for rays traveling toward the thick foil.

Experimental Studies and Numerical Simulations

The new geometries for x-ray-laser targets described in the preceding section were tested on the glass development laser (GDL) single-beam laser system. In all cases the target material was nickel. We have not attempted actual gain measurements because the line-focus lens at our disposal had a length of only 1.5 mm. However, this length was sufficient for studying the hydrodynamic behavior of the proposed new geometries. In the coming months we intend to perform experiments using 1- and 2-cm line-focus lenses, which should yield measurable gain.

The targets were irradiated by 600-ps pulses of 527-nm laser light at intensities of a few 10^{13} W/cm^2. A green-wavelength laser is more suitable than a blue-wavelength laser for exploding-foil experiments because with the shorter wavelength the plasma becomes highly underdense and absorbs less. In the nonexploding geometries, shorter-wavelength illumination is preferable. A cylindrical corrector lens was

fitted onto the f/3 spherical focusing lens to provide a line focus 1.5-mm long and about 50-μm wide at the best focus position. Since a small width may give rise to two-dimensional (2-D) plasma expansion, which would severely degrade the density and temperature profiles, we defocused the beam to yield a width of about 120 μm (at widths larger than 120 μm the intensity distribution across the width is not uniform with the present laser conditions).

Planar nickel foils and slabs were used to construct the target geometries described in the preceding section. The thin foils were 300-Å-thick to 800-Å-thick layers of nickel, supported by Formvar ($C_{11}H_{18}O_5$) substrates 400-Å thick. Such substrates have a very small mass compared with that of the nickel foil and will scarcely affect the hydrodynamic behavior of the foil.

An x-ray crystal spectrometer equipped with a 12-μm entrance slit was used to measure the spatially resolved Ni spectra from these targets in the 7-Å to 14-Å range. The spatial resolution is in the direction perpendicular to the foil plane, which is along the distance between the two foils. These spectra can be used to determine the

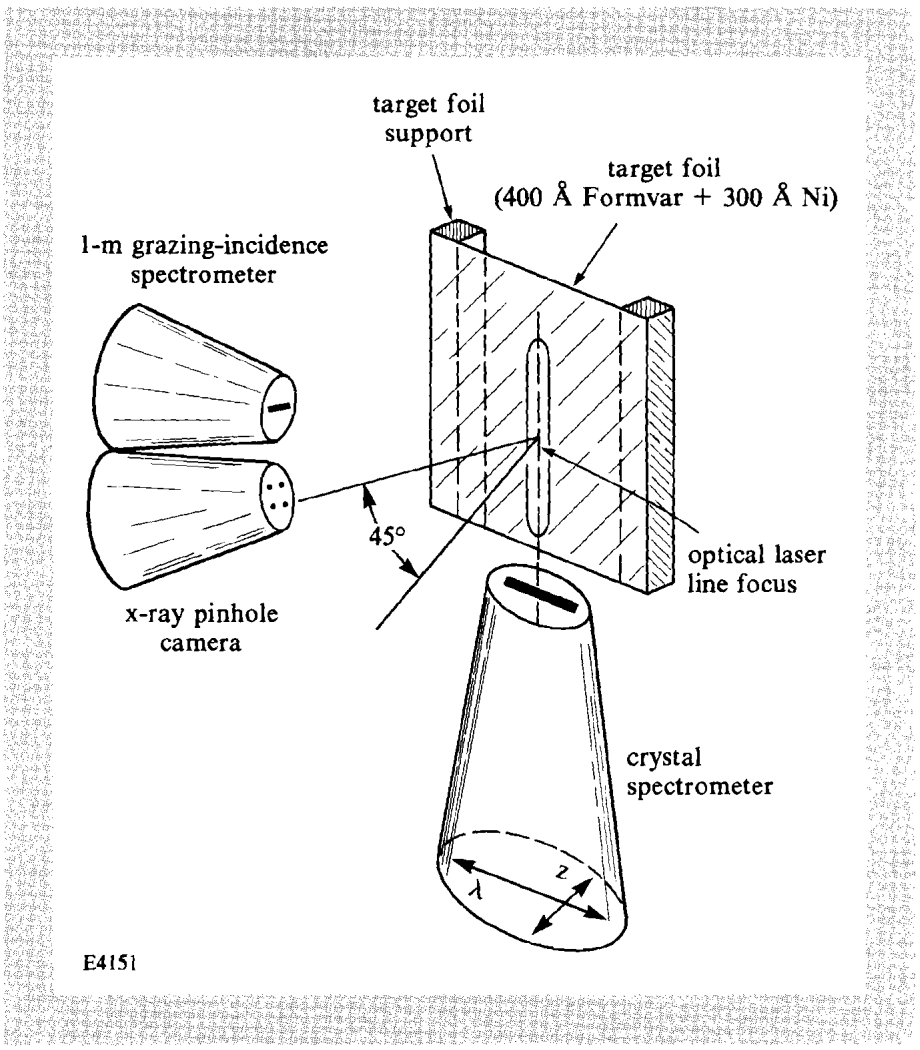

Fig. 30.13
Experimental configuration used for x-ray laser target studies in the GDL target chamber. The crystal spectrometer views the end of the line focus from the bottom. The x-ray pinhole camera and XUV spectrometer view the irradiated side of the target.

plasma temperature and density. Additionally, we used a pinhole camera to measure the focal spot characteristics and also to observe the two-dimensional plasma behavior (along the line focus direction and normal to that direction). This information is important in evaluating the hydrodynamic performance of the new geometries. The XUV spectra in the 40-eV to 250-eV range were measured using a 1-m grazing incidence spectrograph. This spectral range contains the lines that are predicted to lase when using longer line-focus irradiation. Finally, time-resolved measurements of the laser light transmitted through the target were made in order to determine the occurrence of timely burn-through, which is necessary for the formation of a flat density profile.

Figure 30.13 shows the experimental arrangement. The incident laser propagates horizontally and the line focus is oriented vertically. The crystal spectrometer views the plasma along the axis of the line focus. The pinhole camera and XUV spectrometer view the front (irradiated) side of the target at 45° to the normal. The laser light that is transmitted through the target is collected by a spherical *f*/3 lens. The image of the target (along the line focus) is relayed to the slit of a streak camera to obtain time resolution of the transmitted light.

Figure 30.14 shows a typical x-ray spectrum obtained from a thick (about 100-μm) nickel target irradiated at 1×10^{13} W/cm^2. To calibrate the wavelength scale we used a target composed of two

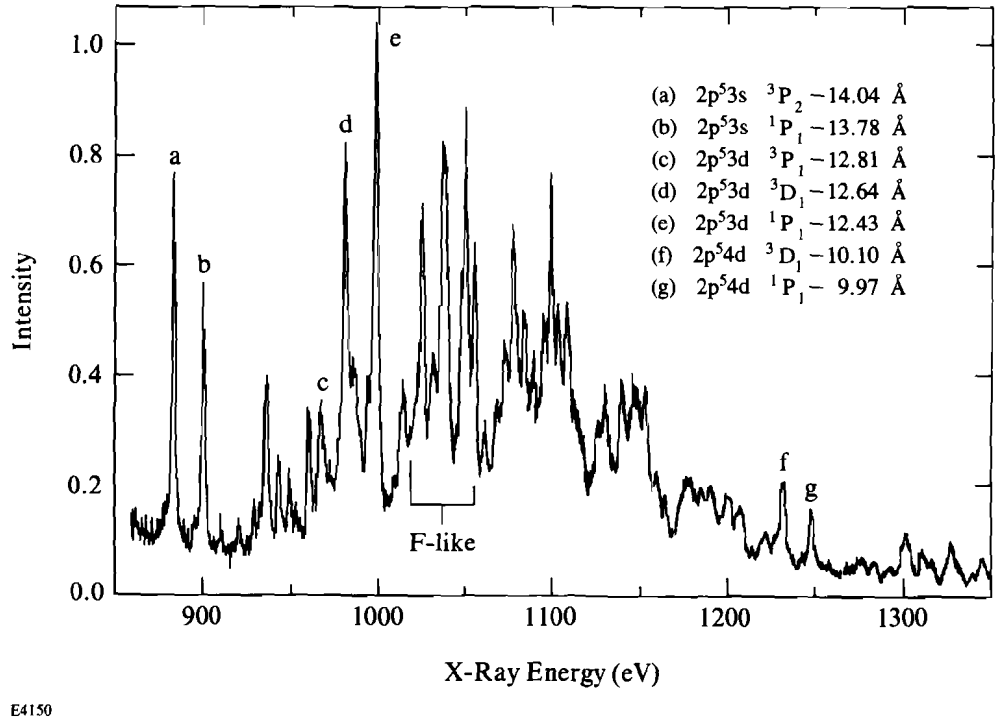

Fig. 30.14
A sample x-ray spectrum from a thick nickel target. The lines designated by letters *a* through *e* are the $n = 3$ to $n = 2$ lines of Ne-like nickel. The lines *f* and *g* are due to $n = 4$ to $n = 2$ transitions. Also indicated are the F-like nickel transitions used in this work. The incident laser intensity was 10^{13} W/cm^2.

regions: nickel and Teflon, irradiated by a line focus. On a spatially resolved spectrum, lines of nickel and fluorine are juxtaposed, thereby providing a reference wavelength scale. Figure 30.14 shows lines from the NiXIX to NiXXII states of ionization (Ne-, F-, O-, and N-like ions). The individual Ne-like and F-like lines can be distinguished, while the emission from the other ionization species appear as unresolved transition arrays. The lines labeled in Fig. 30.14 indicate some of the various Ne-like and F-like lines that were identified using a relativistic atomic structure code.[9] We use the relative intensity of the $2p^6$-$2p^5 3s$ and $2p^6$-$2p^5 3d$ resonance transitions in the Ne-like ions and the analogous $2p^5$-$2p^4 3s$ and $2p^5$-$2p^4 3d$ resonance transitions in the F-like ions to estimate the relative fractional population of these species (from which temperature can be inferred).

In order to determine the thickness of Ni foil required for properly timed burn-through, we started by irradiating single exploding foils of various thicknesses. Figure 30.15 shows spatially resolved spectra (isodensity contours) from three Ni foils of different thicknesses; the substrate in these shots only was a 3000-Å-thick CH layer. In all three cases the laser irradiance was about 3×10^{13} W/cm^2. In Fig. 30.15, the vertical axis is the spectral direction and the horizontal axis is the spatially resolved direction. The laser is incident from the right. Such results indicate whether the target explosion provides an adequate plasma profile for x-ray lasing. For achieving a flat density profile, the foil has to be burned through before the peak of the pulse; in this case, the time-integrated spectrum should be relatively symmetrical (front to back). For too thick a foil, the spectrum is expected to fall much more sharply toward the back of the foil. The spectra in Fig. 30.15 indicate that the 300-Å nickel foil explodes quite symmetrically, whereas the symmetry is gradually degraded for the thicker foils.

One-dimensional (1-D) computer simulations were performed in slab geometry. Since the extent of plasma expansion is of the order of the laser spot width, it is expected that 2-D effects will not markedly change the target behavior. This assumption has been confirmed by 2-D runs that were performed for some of these geometries. Figure 30.16 shows the spatial temperature and density profiles at the peak of the pulse from the 1-D simulations of all three Ni-foil thicknesses shown in Fig. 30.15. These profiles agree qualitatively with the behavior of the foils as exhibited by the time-integrated, spatially resolved spectra; the thinner foil exhibits flat-top density and temperature profiles, whereas the thicker foils show a sharper falloff. A more quantitative comparison with calculated, time-integrated, spatial x-ray profiles of resonance line emission is now in progress.

Figure 30.17 shows the spatially resolved spectrum from a 300-Å Ni foil (supported by a 400-Å CH substrate) irradiated at 1.25×10^{13} W/cm^2. Compared with the spectrum in Fig. 30.15, the use of a lower irradiance and a thinner CH substrate results in a spectrum that shows a higher Ne-like fraction and a more symmetric expansion of the nickel plasma. The experimental results shown in Fig. 30.15 were obtained using a higher irradiance than that required to maximize the Ne-like ion fraction. This is partly due to the use of a relatively thick

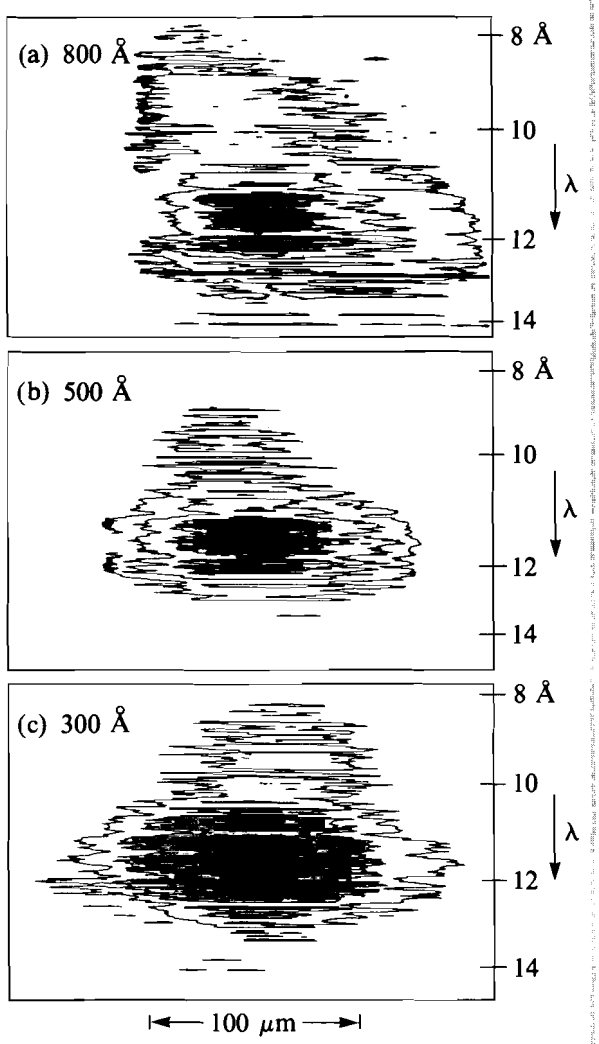

Fig. 30.15
The spatially resolved spectra from three thin-foil targets of various thicknesses: (a) 800 Å Ni, (b) 500 Å Ni, and (c) 300 Å Ni. The spatial axis is transverse to the x-ray laser axis and the wavelength scale is in angstroms, as shown. All targets were supported by 3000 Å of CH and were irradiated by a 0.6-ns pulse at 3×10^{13} W/cm^2. In all figures the optical laser is incident from the right side.

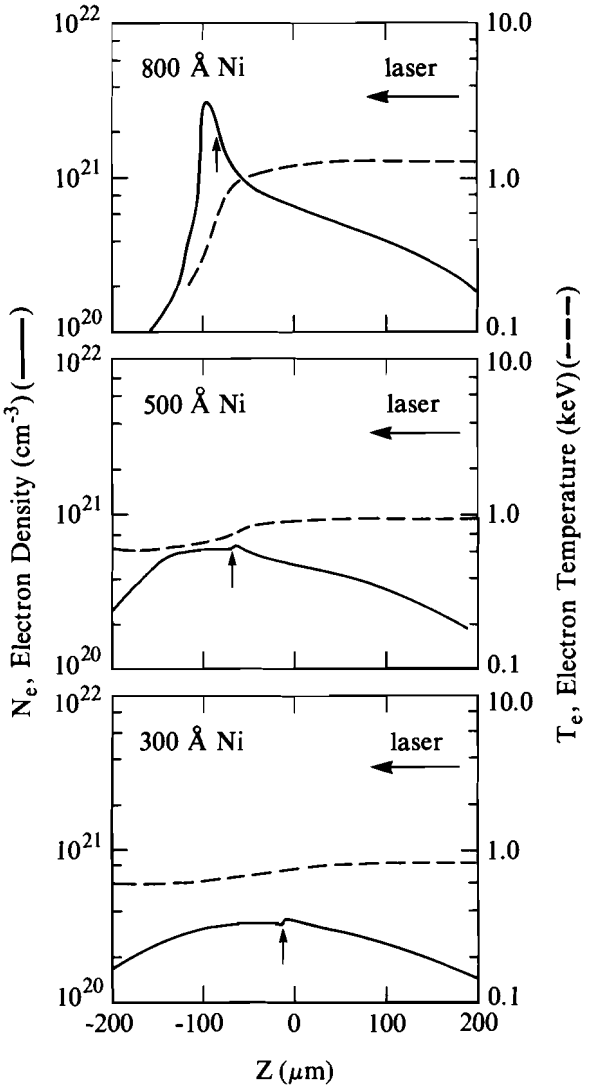

Fig. 30.16
The simulated density and temperature profiles of the targets shown in Fig. 30.15. These profiles are at the peak of a 0.6-ns laser pulse at 3×10^{13} W/cm^2. The optical laser is incident from the right. The arrows indicate the plastic/nickel interface in the targets.

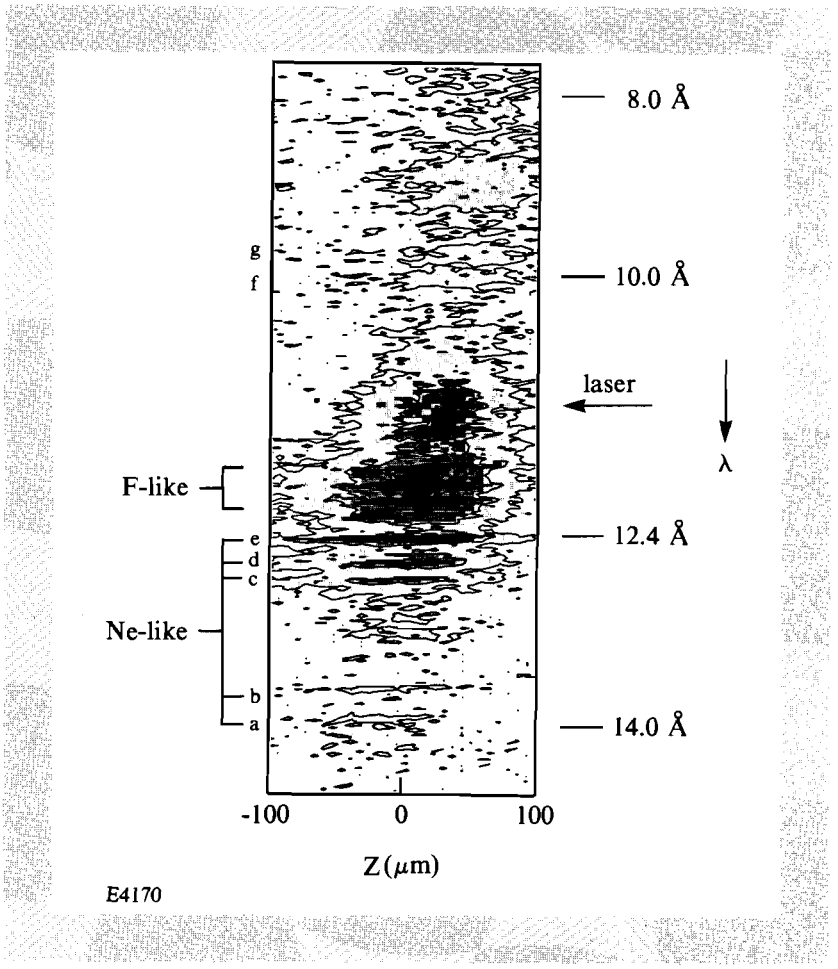

Fig. 30.17
The spatially resolved spectrum of a 300-Å Ni foil (supported by 400 Å Formvar) irradiated by a 0.6-ns pulse at 1.25×10^{13} W/cm^2. The expansion of the plasma can be noted in the various lines of the nickel emission. The seven lines labeled *a* through *g* are the Ne-like transitions shown in Fig. 30.14. Also shown are the two F-like lines indicated in Fig. 30.14.

CH substrate. Our numerical simulations, which used a non-LTE, average-ion, atomic physics model to describe the ionization process, have shown that in order to achieve higher Ne-like ionic fraction and still burn through the foil, we need to use a lower laser intensity and a thinner CH substrate. This finding agrees with the experiments.

We next describe two experiments that employ double thin-foil targets irradiated from one side only. Two foil-separation distances were employed: 120 μm and 270 μm. The nickel coatings were over the inside faces.

Figure 30.18 shows the spatially resolved x-ray spectrum for a separation of 120 μm and an irradiation of 1.1×10^{13} W/cm^2. The plasma expansion is not greater than that exhibited by the single foil illustrated in Fig. 30.17. In Fig. 30.19, the temperature and density profiles from a simulation of this target are compared. These profiles were obtained at -0.1, $+0.2$, and $+0.4$ ns with respect to the peak of the pulse. Figure 30.19 shows that too small a separation distance results in an early collision, leading to a nearly single-foil behavior at later times. A larger separation distance would result in a wider profile. This is particularly important because a single low-Z foil with a subnanosecond laser pulse may result in narrower density profile as compared to a higher-Z foil (a low-Z target requires lower irradiance and thinner foils than needed for higher-Z foils).

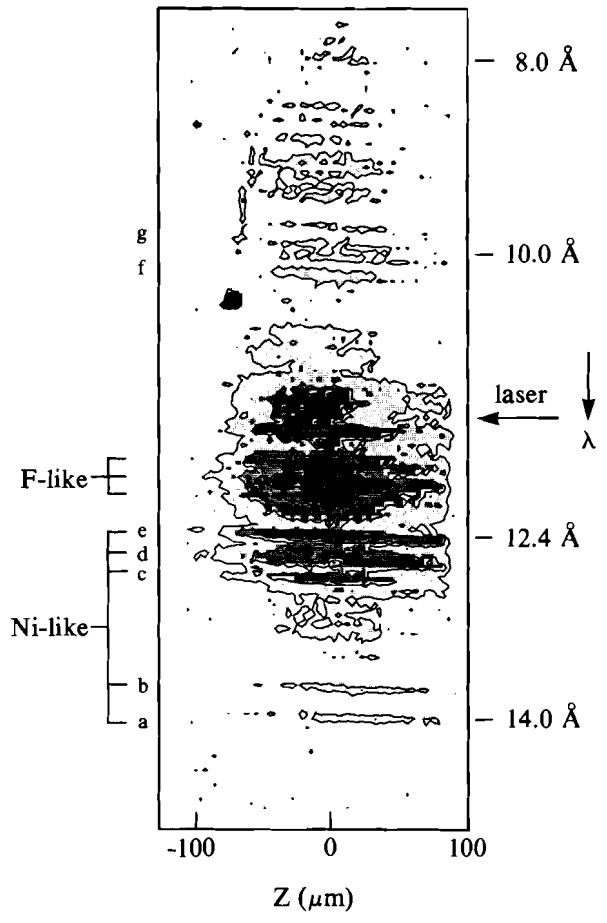

Fig. 30.18
The spatially resolved spectrum of a double thin-foil target consisting of two 300-Å Ni foils (each supported by 400 Å Formvar) and spaced 120 μm apart. The laser intensity was 1.1 × 10^{13} W/cm^2 in a 0.6-ns pulse.

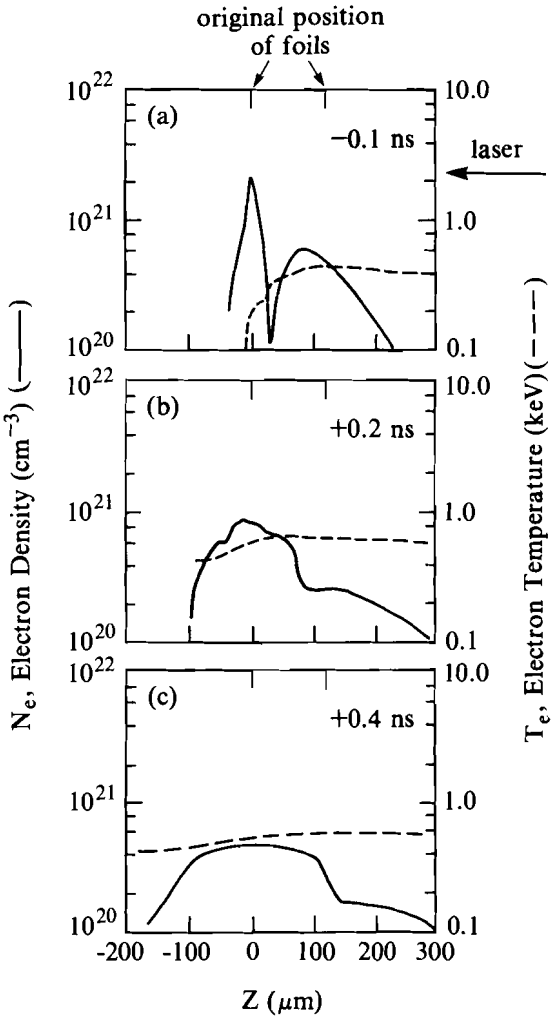

Fig. 30.19
The simulated density and temperature profiles of the double thin-foil experiment shown in Fig. 30.18 at times (a) −0.1 ns, (b) +0.2 ns, and (c) +0.4 ns, relative to the peak of the pulse. An expansion similar to that of a single exploding foil is observed after the collision.

Figure 30.20 shows the spatially resolved x-ray spectrum from a double thin-foil target with a spacing of 270 μm with a laser irradiance of 1.5 × 10^{13} W/cm^2. These two foils were spaced far enough apart so that the individual foil expansions can be discerned in the x-ray spectral image. The sharp diagonal edge on the left of Fig. 30.20 is caused by the edge of the x-ray film. In Figs. 30.21(a)–30.21(c) we

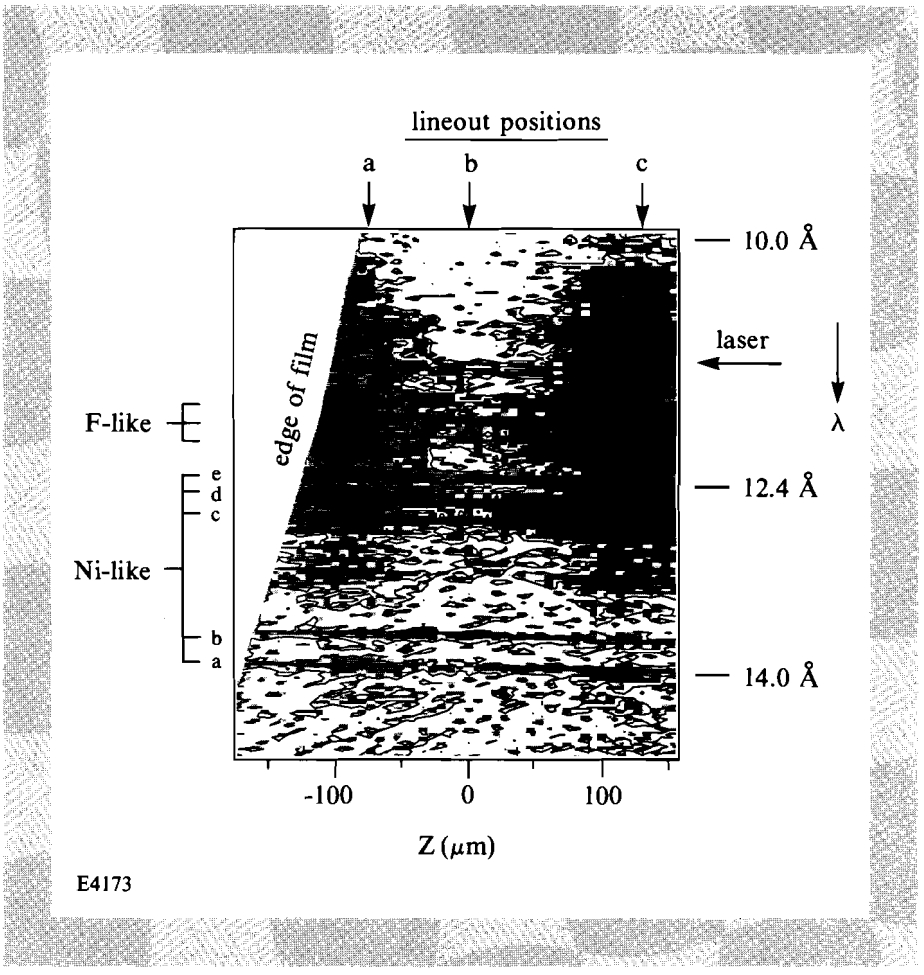

Fig. 30.20
The spatially resolved spectrum of the second double thin-foil target, which consisted of two 300-Å Ni foils (each supported by 400 Å Formvar) spaced 270 μm apart. The laser intensity was 1.5×10^{13} W/cm^2 and was incident from the left in the figure. The sections labeled *a*, *b*, and *c* are the lineouts representing the spectra at the rear foil, at the center, and at the front foil, respectively.

show intensity-corrected spectra at the positions marked *a*, *b*, and *c* in Fig. 30.20 (each spectrum has been normalized to the maximum of spectrum *c*). Note that the spectra at *a* and *c* show significant amounts of Ne-like line emission, whereas in the central region the Ne-like line emission is less pronounced. The ratio of F-like to Ne-like line emission was found to be lower in the central region compared to the ratio near the foils, indicating a lower temperature in that region. In addition, the overall lower intensity in the center indicates a lower density there.

Figure 30.22 shows the temperature and density spatial profiles from a simulation of the target with 270-μm spacing. This set of figures displays the profiles at −0.1, +0.3, and +0.6 ns relative to the peak of the pulse. Figure 30.22(a) shows the initial expansions of the two foils, which exhibit a time delay between the expansions of the two foils because the first foil (right side) is initially opaque to the laser light. In fact, the first foil acts as a shutter and blocks the laser light until its intensity is near peak value. Figures 30.22(b) and 30.22(c) correspond to the times when the two plasmas collide and then relax into a long scale-length plasma, respectively. Figure 30.22(b) is shown to illustrate how the two plasmas coalesce; the exact behavior at this point depends on how the collision of two plasmas is modeled. The

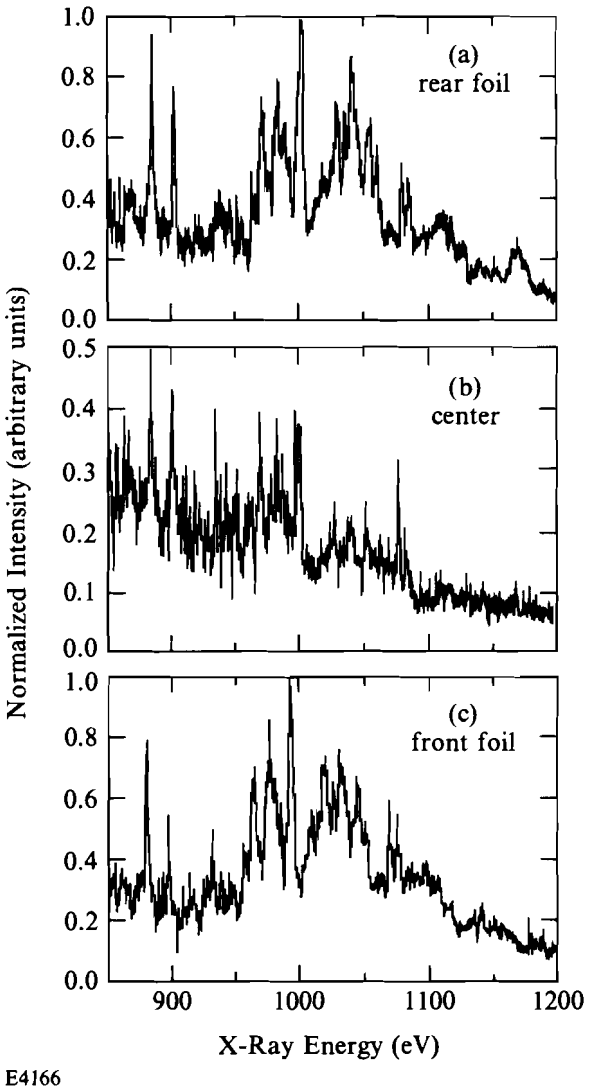

Fig. 30.21
The spectra at various positions in the target shown in Fig. 30.20. The spectra are at (a) the rear foil, (b) the center region, and (c) the front foil. The intensity of each spectrum has been normalized to the peak emission in the spectrum at position *c*. Note that in each foil (spectra *a* and *c*) the spectrum is dominated by Ne-like line emission.

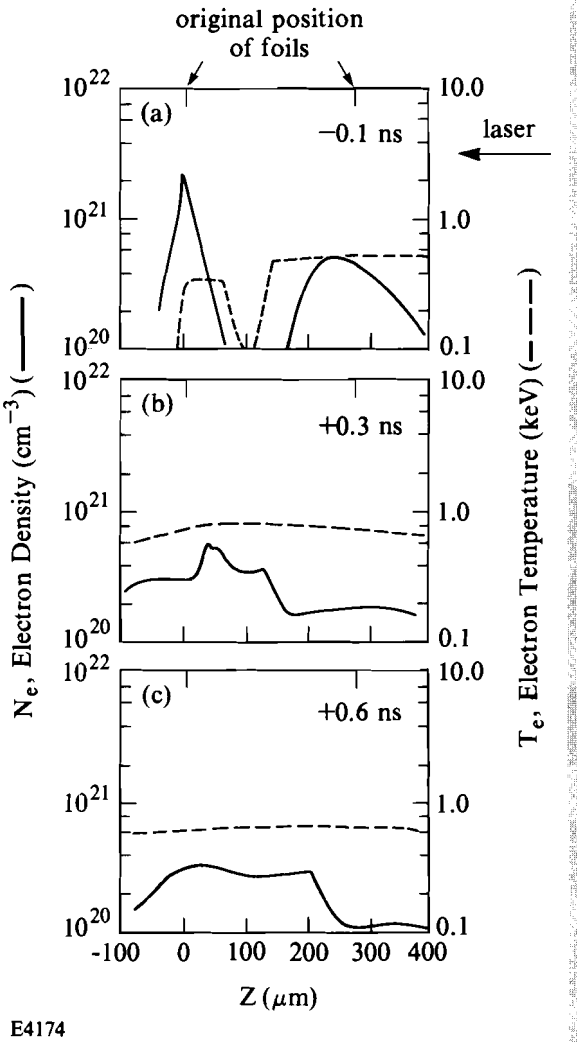

Fig. 30.22
The simulated density and temperature profiles of the double thin-foil experiment shown in Fig. 30.20 at times (a) −0.1 ns, (b) +0.3 ns, and (c) +0.6 ns, relative to the peak of the pulse.

lower measured temperature between the foils can be understood on the following basis: (a) the collision of the two plasmas for this large separation occurs well after the peak of the pulse, when the plasmas are cooler, and (b) 2-D effects, which are important for this foil-separation distance, cause lateral expansion and further cooling.

As mentioned above, one of our goals is to produce a concave density profile of relatively high density. To that end, we studied the behavior of targets that exploit the confinement of an ablated plasma between two thick slabs. Figures 30.23(a)–30.23(d) show the calculated time evolution of the temperature and density profiles for the double-slab target at four different times. In this simulation, the laser light is normally incident on both inner surfaces of the parallel slabs, at an intensity of 1.75×10^{13} W/cm^2 on each surface. The figures show the rising density of the plasma, which eventually fills

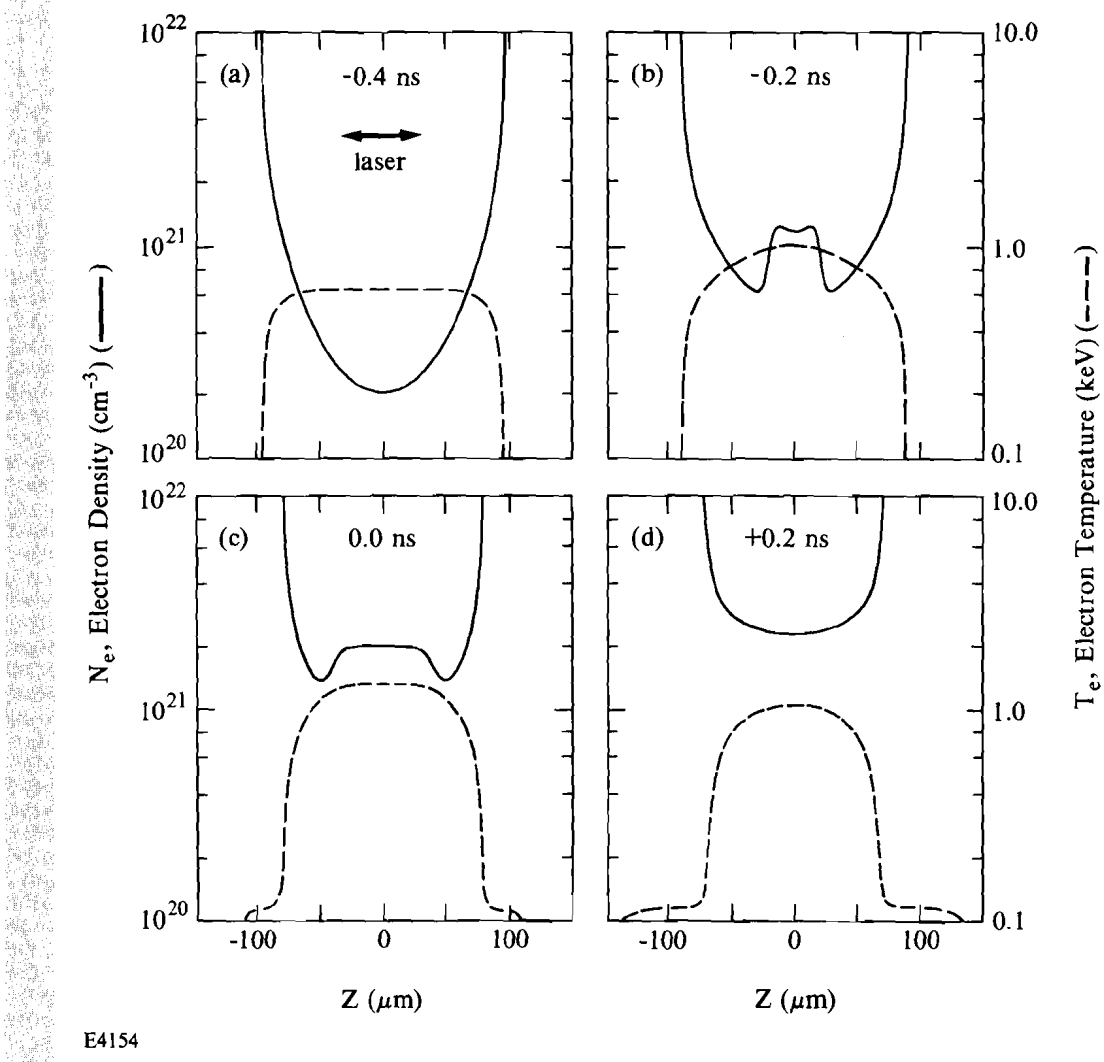

Fig. 30.23
The simulated density and temperature profiles of the double thick-foil ablative-plasma target shown conceptually in Fig. 30.12(c). The profiles are shown at times (a) −0.4 ns, (b) −0.2 ns, (c) 0 ns, and (d) +0.2 ns, with respect to the peak of a 0.65-ns pulse of 527-nm light at 1.75×10^{13} W/cm^2 irradiating each of the two foils. In (b), the collision of the two ablated plasmas begins to increase the density in the interfoil space, followed by a continuously growing density, as seen in (c) and (d).

the interfoil space. The plasma temperature is uniform across the gap at about 1 keV (for nickel, a lower temperature is actually required).

Two simplified versions of this target geometry, suitable for the single-beam GDL experiments, were investigated. The first version involves two thick (>100-μm) Ni foils 300 μm apart, one of which was irradiated on its inner surface. Figure 30.24 shows the pinhole camera image of this target, irradiated at about 5×10^{13} W/cm^2. The outline of the incident beam is shown for reference, as are the positions of the two slabs. Heating of the inner side of the second foil (by the ablated plasma and possibly by the reflected light from the laser-irradiated foil) can be seen. This preliminary result demonstrates the ability to create a plasma throughout the gap with only one laser beam. Additional studies are under way to optimize this configuration.

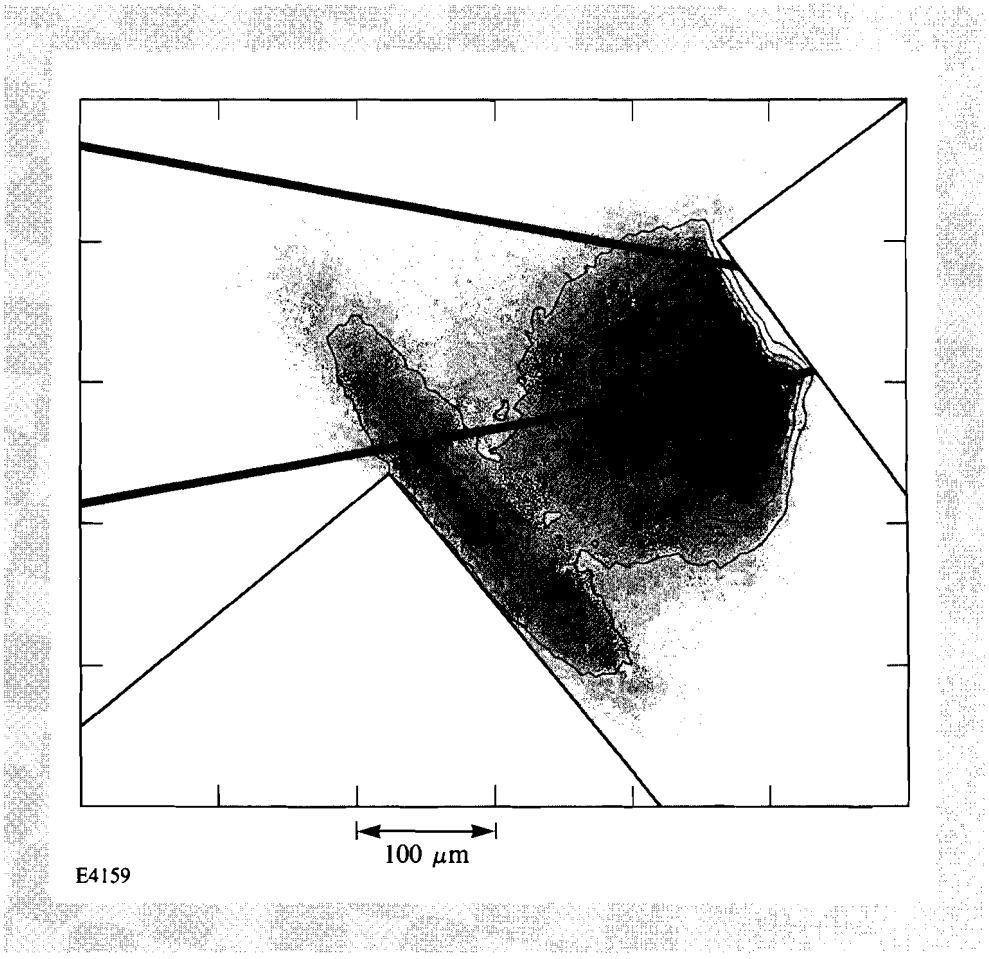

Fig. 30.24
The pinhole image (end on) of a double thick-foil target irradiated by a single laser beam that is incident from the left (the outline of the beam is shown in the figure). The incident intensity is about 5×10^{13} W/cm^2. For this image, the pinhole camera was placed in the position of the crystal spectrometer shown in Fig. 30.13.

The second simplified version of the target described in Fig. 30.23 was a combination of a thin (300-Å Ni+ 400-Å CH) foil and a thick (>100-μm) Ni foil. The thin foil was positioned with the nickel coating on the side facing the nickel slab. The laser was incident on the outer side (CH support) of the thin foil. Figure 30.25 shows the spatially resolved x-ray spectrum from this target irradiated at 1.5×10^{13} W/cm^2. The plasma created by this target has about the same spatial extent as that of the superposition of the observed plasmas from

a thin and a thick target separately. The addition of a thin foil in front of a thick foil has the effect of creating a density plateau on the otherwise sharply falling density profile of the thick foil. The ratio of Ne-like to F-like line emission as a function of space indicates that the temperature is approximately constant between the foils and that the increased x-ray emission (due to the addition of the thin foil) is mainly the result of increased density.

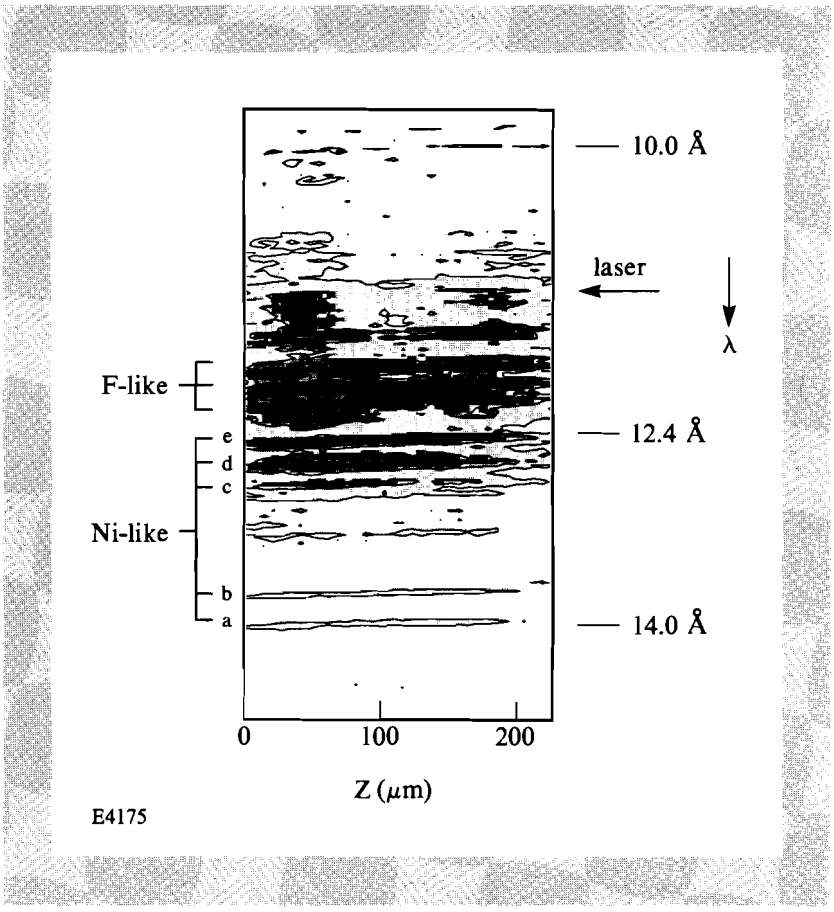

Fig. 30.25
The spatially resolved spectrum of a double-foil target that consisted of a 300-Å Ni foil (supported by 400 Å Formvar) and a 100-μm-thick Ni foil spaced 240 μm apart. The laser intensity was 1.5×10^{13} W/cm^2 and was incident from the right of the figure. A nearly constant emission can be seen in the region between the original foils.

In Fig. 30.26 we show the simulated temperature and density profiles for this target shot at various times relative to the peak of the pulse. They show that the density profile of the ablated plasma from the thick slab is flattened by the presence of the thin exploding foil.

Figure 30.27 summarizes the performance of the new geometries in these experiments. It shows the measured intensity of the Ne-like $2s^22p^6$-$2s^22p^53d$ line (at 12.4 Å) for the various targets described above. All the curves in this figure have the same scale. The laser energy was different in these experiments, but indications from the simulations indicate that the absorbed energy differences were smaller. Comparison of the two lower curves shows that two foils that are too closely spaced behave essentially like a single foil (the slightly wider profile of the single foil can be attributed to the different laser energy). Three features are particularly notable in this figure: (1) the plateau exhibited by the target having one thin and one thick foil; (2) the wide

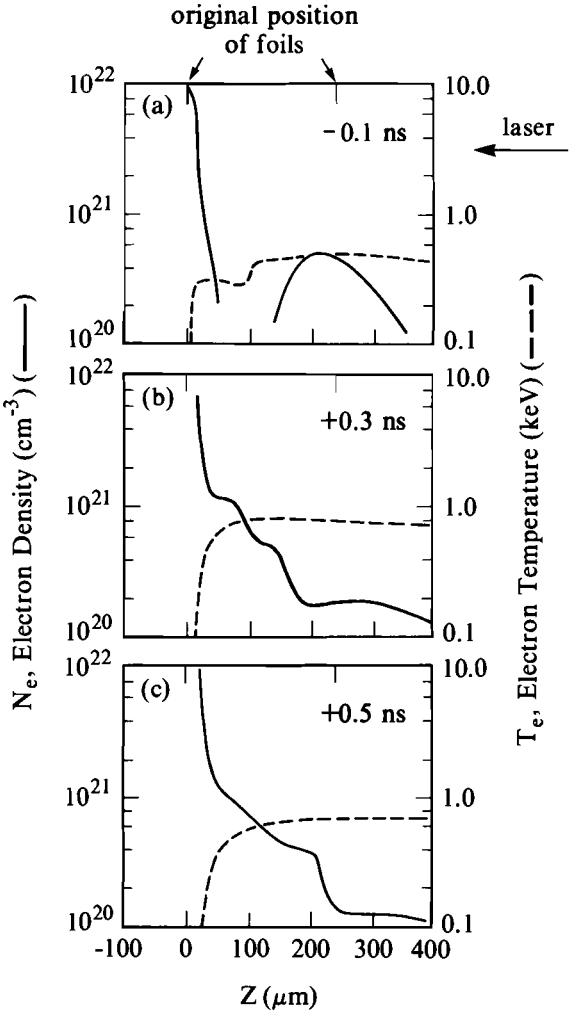

Fig. 30.26
The simulated density and temperature profiles of the double-foil experiment shown in Fig. 30.25. The profiles are shown at times (a) −0.1 ns, (b) +0.3 ns, and (c) +0.5 ns, relative to the peak of the pulse. Noteworthy is the flattened region [(b) and (c)] formed in the density profile from the presence of the single-foil plasma expansion. This behavior is confirmed by the spatially resolved emission shown in Fig. 30.25.

and concave profile in the target having two widely spaced thin foils; and (3) the higher intensity from both of these targets (as compared with a thin target) is indicative of a higher density. These encouraging results should enable the achievement of efficient amplification in future x-ray laser experiments.

ACKNOWLEDGMENT

This work was supported by the Naval Research Laboratory under contract No. N00014-86-C-2281.

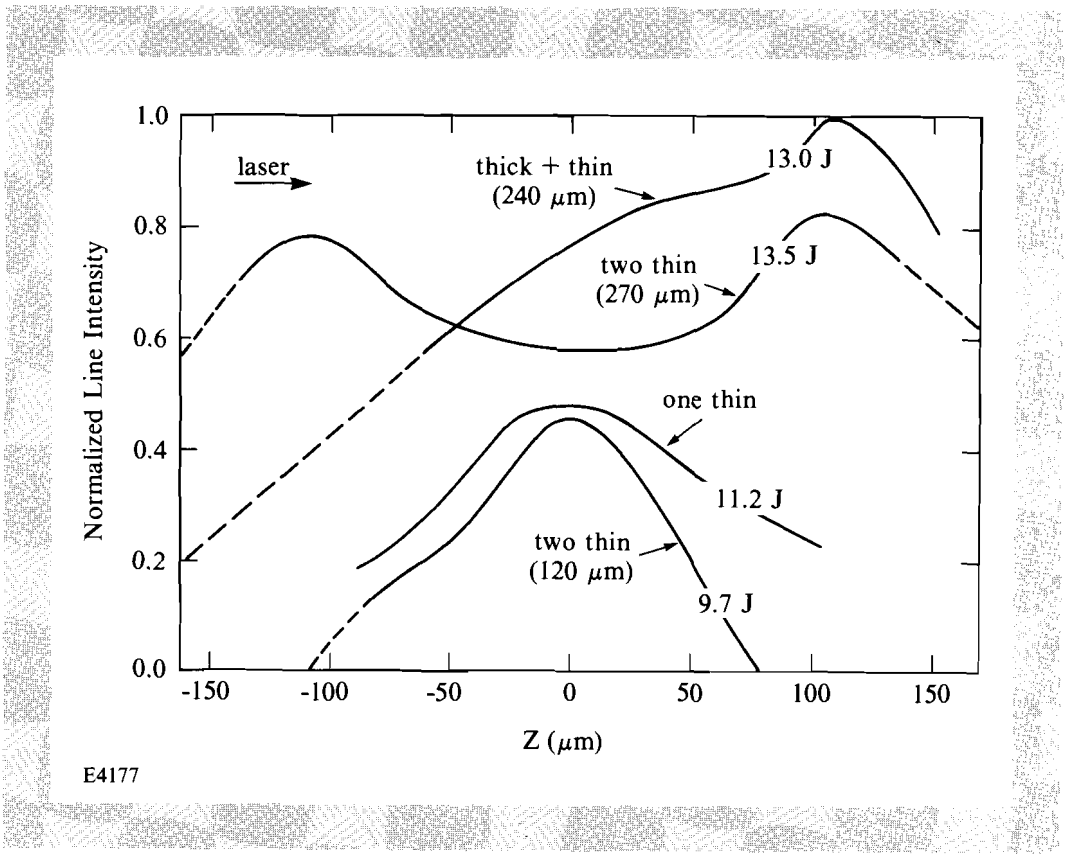

Fig. 30.27
A comparison of the measured intensity of the Ne-like $2s^22p^6 - 2s^22p^53d$ line (denoted by *e* in Fig. 30.14) for the various targets described above. The curves are plotted on the same scale, but each target has a different irradiated intensity (the laser energy used at each case is specified; the intensity at each case is proportional to the laser energy). This figure shows the relative performance of the various targets to produce large regions of Ne-like ion populations that can be used as x-ray-laser gain media.

REFERENCES

1. M.D. Rosen *et al.*, *Phys. Rev. Lett.* **54**, 106 (1985).
2. D. L. Matthews *et al.*, *Phys. Rev. Lett.* **54**, 110 (1985).
3. Energy and Technology Review, Lawrence Livermore National Laboratory Report UCRL-52000 (1985), p.1.
4. Recently, A. Bar-Shalom of NRCN (Israel) has calculated population inversion on the $2s2p^63d$-$2s2p^63p$ transition (which, for neon-like nickel, is at 242 Å; see Fig. 30.11); here, a 2*s* electron, rather than a 2*p* electron, is excited.
5. U. Feldman, J. F. Seely, and A. K. Bhatia, *J. App. Phys.* **56**, 2475 (1984).
6. M. D. Rosen and P. L. Hagelstein, Lawrence Livermore National Laboratory Report UCRL-94412 (1986).
7. J. P. Dahlburg *et al.*, *Phys. Rev. A* **35**, 2737 (1987).
8. M. C. Richardson, R. Epstein, O. Barnouin, P. A. Jaanimagi, R. Keck, H. Kim, R. S. Marjoribanks, S. Noyes, J. M. Soures,

and B. Yaakobi, *Phys. Rev. A* **33**, 1246 (1986); M. C. Richardson, B. Yaakobi, R. Epstein, J. S. Wark, and J. M. Soures, *High-Intensity Laser Processes* (SPIE, Bellingham, WA, 1986), Vol. 664, p. 270.

9. M. Klapisch *et al.*, *J. Opt. Soc. Am.* **67**, 148 (1977); M. Klapisch, *Comp. Phys. Comm.* **2**, 239 (1971).